RSC Advances

PAPER

View Article Online
View Journal | View Issue

Cite this: *RSC Adv.*, 2025, **15**, 22605

A simple method for Mn residue utilization for efficient peroxymonosulfate activation: enrichment of metal sites and oxygen vacancies *via* alkali-reduction treatment†

Jujiao Zhao,[a] Xianjuan Xu,[a] Qiao Zhang,[a] Feilan Qi,[a] Haoxuan Wei,[b] Quanfeng Wang,*[b] Youzhou He,[a] Xiaoxia Bai,[a] Shun Guan,[a] Ming Zhu[c] and Xingmin Wang*[a]

Transforming Mn residues into catalysts for activating peroxymonosulfate (PMS) for the degradation of organic pollutants is a promising method that could not only mitigate environmental pollution caused by Mn residues, but could also provide inexpensive catalysts for PMS-based wastewater treatment. Herein, a two-step method involving alkali-reduction treatment is proposed for improving the catalytic activity of Mn residues. The proposed alkali treatment successfully reduced the content of Si from 261.0 mg g^{-1} to 80.5 mg g^{-1}, leading to relatively increased contents of Fe and Mn. Moreover, alkaline $NaBH_4$ reduction treatment introduced more oxygen vacancies, further enhancing the performance. The sample treated with the two-step method exhibited rhodamine B (RhB) degradation kinetics of 0.034 min^{-1}, which was 2.43 times higher than that of the control sample. Quenching experiments and electron paramagnetic resonance demonstrated the vital role of $^1O_2$ in the degradation of RhB, and the mechanism was investigated. Furthermore, 18 types of degradation intermediates were detected, and the possible degradation pathway for RhB was proposed. Through employing a toxicity estimate software tool, it is indicated that RhB toxicity continuously decreases during RhB degradation. The findings of this work could shed light on the reutilization of Mn residues and the development of inexpensive catalysts for PMS-based wastewater treatment.

Received 15th February 2025
Accepted 12th June 2025

DOI: 10.1039/d5ra01113b

rsc.li/rsc-advances

1. Introduction

Manganese (Mn) residues, as typical by-products of various industrial activities, such as mining and metallurgical processes, present substantial environmental challenges.[1,2] The accumulation of these residues can lead to the release of heavy metals and other pollutants into the environment, contaminating soil, surface water, and groundwater.[3,4] Without appropriate methods for disposing of Mn residues, serious risks could be posed to ecosystems and human health.[5] Particularly, in China, the stock of Mn residues now exceeds 150 million tons and is escalating at an approximate rate of 10 million tons annually, thereby necessitating the urgent need for the effective management of Mn residues.[6]

"Treating waste with waste" is a desired approach to solve environmental problems.[7,8] Mn residues still contain a certain amount of Fe and Mn, both of which are regarded as chemical active species in advanced oxidation processes (AOPs), which are widely used for removing organic pollutants from wastewater.[9–12]

As one of the AOPs, peroxymonosulfate (PMS) activation has attracted much attention. With suitable catalysts, PMS can produce multiple types of reactive oxygen species (ROS), including sulfate radicals ($SO_4^{\cdot-}$), hydroxyl radicals ($^{\cdot}OH$), and singlet oxygen ($^1O_2$), indicating its good capability in degrading a wide range of organic pollutants, from pharmaceuticals to dyes and pesticides.[13–19] Many efforts have been dedicated to the development of innovative catalysts with outstanding performance for activating PMS.[20] However, the widespread application of PMS activation is still limited by the high cost of catalysts, and most previous studies have either struggled to scale up their proposed processes or utilized intricate precursors for synthesis.[21,22]

The utilization of Mn residues as catalysts for PMS activation is highly desired since this approach converts waste materials

[a]College of Environment and Resources, Chongqing Technology and Business University, Chongqing, 400067, PR China. E-mail: wxm0826@ctbu.edu.cn; Tel: +86-18046504243

[b]School of Civil and Hydraulic Engineering, Chongqing University of Science and Technology, Chongqing, 401331, PR China. E-mail: 2021020@cqust.edu.cn; Tel: +86-13527536325

[c]Institute for Smart City of Chongqing University in Liyang, Chongqing University, Jiangsu, 213300, PR China

† Electronic supplementary information (ESI) available. See DOI: https://doi.org/10.1039/d5ra01113b

into valuable resources for environmental remediation, thus aligning with sustainability principles.[23] Several studies have shown that Mn residues can effectively activate PMS for pollutant degradation, leveraging the catalytic properties from the manganese and iron present in the residues.[24] In this field, He *et al.* and many other researchers have conducted some remarkable studies.[3,25–29] For instance, in one study a modified manganese slag/PMS system could remove 100% of diethyl dithiocarbamate in 10 min.[30] Also, washing manganese slag by both Na_2CO_3 and HNO_3 under optimized conditions led to a levofloxacin removal efficiency of 82.6% within 60 min by activating PMS.[31] In another study, after calcinating Mn residues in air and subsequently treating the sample with H_2SO_4, the obtained catalysts could degrade 85% of tetrachlorophenol within 50 min.[32] Nevertheless, most of these studies employed an acid-washing process to clean the surface and expose more active sites by removing impurities.[7] However, acid washing will result in the leaching of Mn and Fe, which are crucial active sites in the catalyst.[33,34] Additionally, the acid-washing process can be environmentally detrimental due to the generation of acidic waste streams that require further treatment.

To overcome the limitations associated with acid washing, alkali washing has emerged as a promising alternative process to enhance the activity of Mn residues.[35] Alkali washing can remove inert composites such as SiO_2, which has been revealed to be the main component in many Mn residues, while simultaneously preventing the leaching of Fe and Mn.[4,35]

Additionally, several studies have reported that $^1O_2$ could be generated by PMS activated with Mn residues-derived catalysts.[28,29] $^1O_2$ is considered to be a highly active agent for attacking organic pollutants with an electrophilic nature, contributing to the degradation of various organic pollutants.[16,36,37] The generation of $^1O_2$ was speculated to be associated with the existence of oxygen vacancies on the catalysts,[16,38,39] thereby making the enhancement of oxygen-vacancy formation a promising method to further optimize the performance of Mn residues-derived catalysts.[28,40]

Herein, Mn residues were treated by alkali treatment and subsequently treated by alkaline $NaBH_4$ solution to enhance the formation of oxygen vacancies,[40,41] and the obtained catalysts were then used to active PMS for removing rhodamine B (RhB), a typical organic pollutant that is widely used in the world but is harmful to human health.[42,43] Both alkali treatment and alkaline $NaBH_4$ reduction treatment enhanced the performance of the samples and $^1O_2$ was identified to be the main ROS involved. The catalytic mechanism for the degradation of rhodamine B was investigated and the intermediates during the degradation of RhB were revealed. Besides, toxicity assessment was also performed using the toxicity estimate software tool (T.E.S.T.).

2. Experimental

2.1 Chemicals and materials

Mn residues were obtained from companies in Xiushan, Chongqing. 2,2,6,6-Tetramethyl-4-piperidone (TEMP) and rhodamine B (RhB) were obtained from Aladdin Ltd. (Shanghai, China). Absolute ethanol (C_2H_5OH, 99.7%), sodium hydroxide (NaOH, >98%), sulfuric acid (H_2SO_4, 98%), methanol (CH_3OH, 99.7%), L-histidine, sodium chloride (NaCl, 98%), sodium borohydride ($NaBH_4$, 98%) and sodium dihydrogen phosphate (NaH_2PO_4, 98%) were obtained from Chongqing Chuandong Co. These chemicals were used as received without any further purification. The river water was taken from the Chongqing section of the Yangtze River. The lake water was obtained from Cuihu Lake in the campus of Chongqing Technology and Business University.

2.2 Preparation of the samples

The collected Mn residues without any treatment were named as MS.

In a typical process, MS was first calcined at 350 °C in air for 3 h and then washed by water. The obtained sample was then milled into a powder. Then, 10 g calcined MS powder was dispersed in 100 mL of 4 mol per L NaOH solution for 1 h at a temperature of 60 °C. After that, the sample was washed by water and further calcined at 500 °C for 3 h with increasing the temperature at a rate of 5 °C min^{-1}. The alkali-treated and calcined sample was denoted as ACMS.

Another sample was prepared and treated by the similar calcination process but without the alkali treatment for contrast group and this was denoted as CMS.

The ACMS was further treated by alkaline $NaBH_4$ solution to improve its performance. In a typical process, 1 g ACMS sample was immersed in 500 mL 200 mmol per L alkaline $NaBH_4$ solution (pH 11, room temperature) for 150 s and filtrated immediately. The obtained sample was then dried at 60 °C and denoted as ACMS-R.

CMS was also treated by the same process to obtain another sample, which was denoted as CMS-R.

2.3 Characterization methods

The morphology of the samples was observed using a ZEISS Sigma 300 scanning electron microscopy (SEM) system. Transmission electron microscopy (TEM) images were collected on a Talos F200S instrument. Energy-dispersive X-ray spectroscopy (EDS) elemental mapping was performed using the same TEM equipment. X-ray diffraction (XRD) patterns were obtained on a Rigaku Ultima IV (Japan) at a scan rate of 2° min^{-1}. X-ray photoelectron spectroscopy (XPS) analysis was conducted on an ESCALAB 250Xi spectrometer (USA), using an Al Kα X-ray source (1486.6 eV). N_2 adsorption–desorption isotherms were recorded on a Micromeritics ASAP2460 system (USA) and degassing was performed at 200 °C for 8 h. Electron paramagnetic resonance (EPR) measurements were performed using a Bruker EMXmicro-6/1/P/L instrument with TEMP as the spin-trapping agent. Inductively coupled plasma-atomic emission spectrometry (ICP-AES) was performed using a PerkinElmer Optima 5300 DV instrument.

2.4 Procedures and analysis

A 250 mL beaker was used as the reactor and a 100 mL solution of 50 mg L^{-1} RhB was added to the beaker. A magnetic stirrer was employed at a stirring speed of 400 rpm to evenly disperse

the catalysts during the process. The temperature was controlled by the heating function of the magnetic stirrer. The pH was adjusted by adding NaOH or H_2SO_4. The reaction time was recorded and the count started after the addition of PMS. The solution samples for detection were collected and filtered through a 0.22 μm filter. Next, 0.5 mL quenching solution mixed with methanol and L-histidine was added into the sample to terminate the oxidation reaction. The concentration of RhB was detected by UV-vis spectroscopy (UV2365, UNICO, Shanghai, China) at 554 nm. The degradation intermediates of RhB were identified by liquid chromatography-mass spectrometry (LC-MS) (Agilent LC1290-6550-QTOF with a C-18 column, mobile phase: acetonitrile/water (60 : 40, v/v), flow rate: 0.3 mL min^{-1}). The total organic carbon (TOC) removal efficiency was revealed using a Shimadzu TOC-L-CPH system. The toxicity estimate software tool (T.E.S.T.) was employed to evaluate the change of toxicity during the degradation of RhB.

3. Results and discussion

3.1 Characterization of the catalysts

The SEM images with different magnifications of CMS, ACMS, and ACMS-R can be seen in Fig. 1. The SEM images of CMS (Fig. 1a and b) show the presence of many cracks with a rugged structure. The larger magnification image shows the morphology consisted of nanoparticles. ACMS, the sample prepared with the alkali-washing step, presented a much similar structure. After the alkali-reduction treatment by $NaBH_4$ solution, the structure of ACMS-R also did not change much. TEM images of ACMS-R were also recorded (Fig. S1†), which further demonstrated that ACMS-R exhibited a nanoparticles structure.

The EDS elemental mapping provided further insight into the compositional homogeneity of the ACMS-R. A uniform distribution of Mn and Fe could be observed in the ACMS-R sample, as depicted in Fig. 2. Since Mn and Fe were regarded as the active elements for activating PMS, this uniformity could be favorable for the activity of the catalysts.

The phase composition of the samples was revealed by XRD measurements, as shown in Fig. 3a. The preponderant crystalline structures of CMS were SiO_2 (JCPDS. 70-3755), $Ca_3Si_2O_7$ (JCPDS. 22-0539) and $CaSO_4$ (JCPDS. 72-0916). Generally, these substances are regarded as having poor catalytic activity toward PMS activation.[32] After alkali treatment, the signals for $CaSO_4$ disappeared in the XRD pattern of ACMS; meanwhile, peaks corresponding to $CaFe_5O_7$ (JCPDS. 30-0257) and $CaMn(Si_2O_6)$ (JCPDS. 74-0336) could be observed. It is worth noting that $CaSO_4$ could react with NaOH, leading to the recrystallization of Ca ions. On the other hand, the intensity of diffraction peaks of the quartz phase materials might then be reduced, resulting in the observation of the peaks corresponding to Fe, Mn-containing substances. However, the XRD pattern of ACMS-R was exactly similar to that of ACMS, indicating the alkali-reduction treatment by $NaBH_4$ solution did not change the crystalline structure of the samples. The N_2 adsorption–desorption isotherms of CMS, ACMS, and ACMS-R are depicted in Fig. 3b and the Brunauer–Emmett–Teller (BET) surface area was calculated. CMS, ACMS, and ACMS-R exhibited BET surface areas of 13.5, 15.1, and 18.5 $m^2 g^{-1}$, respectively. These results revealed the increase in the BET surface area after alkali treatment and alkaline $NaBH_4$ solution treatment. A larger BET surface area will increase the contact area for capturing PMS molecules, which could facilitate the degradation efficiency of organic pollutants with PMS activation.

Alkali treatment was expected to reduce the content of inactive materials and avoid the leaching of Mn and Fe. To further reveal is this was true, ICP-AES was employed and the contents of Mn, Fe, and Si in MS, CMS and ACMS were investigated, and the results can be seen in Table S1.† MS contained a high concentration of *S* (1527.9 mg g^{-1}), which was in the form of soluble sulfates, leading to relatively lower contents of the other elements. Significantly, the content of Si decreased from 261.0 mg g^{-1} to 80.5 mg g^{-1}, while the contents of Fe and Mn in ACMS were obviously higher than those in CMS. These results demonstrate that the alkali treatment could reduce the content of Si element, leading to the increased relative contents

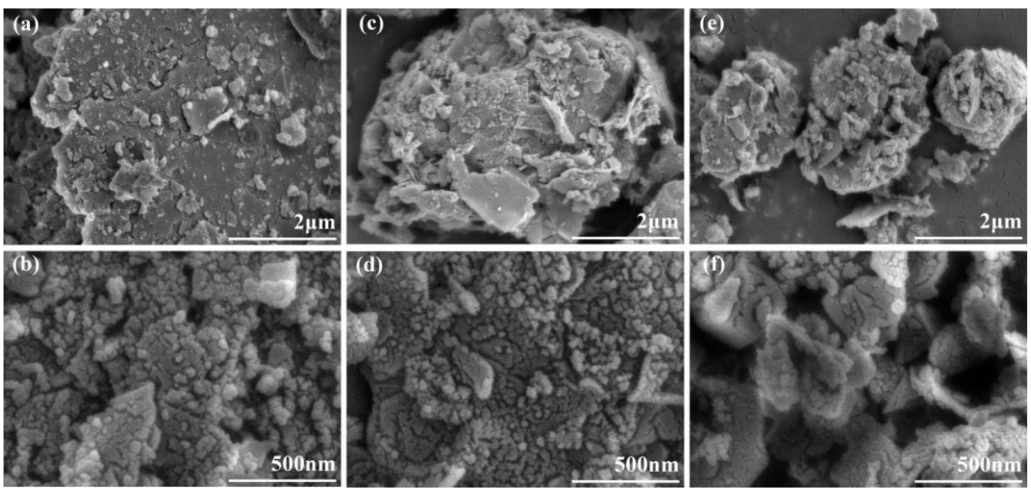

Fig. 1 (a) and (b) SEM images of CMS; (c) and (d) SEM images of ACMS; (e) and (f) SEM images of ACMS-R.

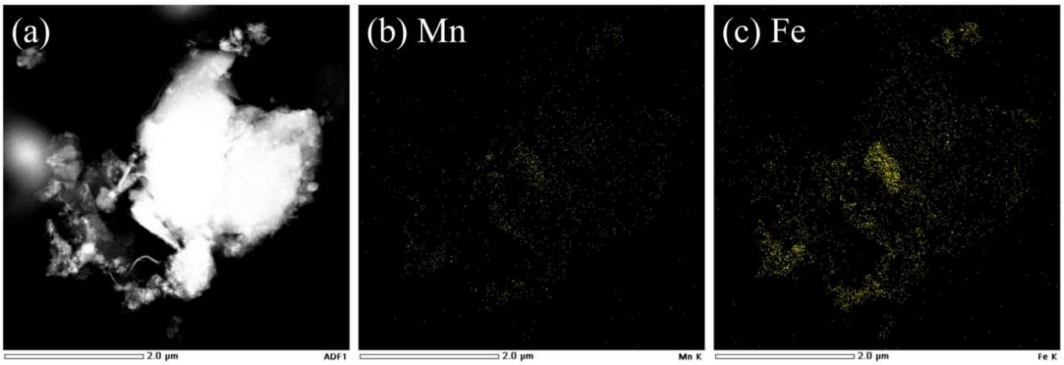

Fig. 2 (a)–(c) EDS elemental mapping images of ACMS-R.

of Fe and Mn, both of which are regarded as active in PMS activation.

The detailed element information of the samples was investigated by XPS. As shown in Fig. 4a, the Fe $2p_{3/2}$ peak could be deconvoluted into two peaks at 710.6 and 712.6 eV corresponding to Fe^{2+} and Fe^{3+}, respectively.[29] The Fe^{2+}/Fe^{3+} ratios of CMS, ACMS, and ACMS-R were 62.3 : 37.7, 46.2 : 53.8, and 56.6 : 43.4, respectively. After the alkali treatment, the ACMS sample presented a lower Fe^{2+} content compared to CMS. The alkali treatment reduced the content of Si element and resulted in the reconstruction of the metal species, which might facilitate the oxidation of Fe species. With further treating ACMS with alkaline $NaBH_4$ solution, the Fe^{2+} content in the ACMS-R sample increased, which could be due to the reductive ability of $NaBH_4$. A similar trend could also be observed in the valence conversion of Mn in the samples. As depicted in Fig. 4b, the Mn $2p_{3/2}$ spectra of the three samples could be deconvoluted into three peaks corresponding to Mn^{2+} (641.0 eV), Mn^{3+} (642.2 eV), and Mn^{4+} (644.3 eV), respectively.[28,29] The Mn^{2+} content of ACMS-R was 50.7% of the total Mn, which was much higher than that of ACMS (28.6%). The O 1s spectra of ACMS and ACMS-R can be seen in Fig. S2.† The observed peak at 529.7 eV could be due to the oxygen in the lattice (O_L).[28,29] The peak at 531.6 eV could be attributed to the oxygen atoms with a low coordination toward metal ions, which originated from the existence of oxygen vacancies.[12,44] Thus, these kinds of oxygen atoms are regarded as O_V in this manuscript. The peak at 532.7 eV represented the oxygen in the adsorbed molecules (O_{ads}) on the surface (such as H_2O).[14,44] The O_V/O_L ratio of ACMS was 4.14, while that value for ACMS-R was 4.75. The increased O_V/O_L ratio indicated the successful formation of more oxygen vacancies during the alkali-reduction treatment by $NaBH_4$ solution, which was in accordance with previous reports.[41]

3.2 Catalytic performances of the samples

The catalytic performances of the prepared samples were investigated by degrading RhB under similar conditions, as shown in Fig. 5 and S3.† The oxidation of RhB by PMS alone was first evaluated and 27.7% of RhB was removed within 30 min. The adsorption of ACMS-R was next investigated and ACMS-R could only adsorb a small amount of RhB (1.6%), demonstrating the removal of RhB mainly depended on the oxidation process. As displayed in Fig. 5a, by adding CMS as the catalyst, merely 32.2% of RhB was removed within 30 min, revealing the poor activity of CMS for PMS activation. ACMS, the sample prepared with alkali treatment, presented a RhB removal efficiency of 56.5% within 30 min, which was significantly higher

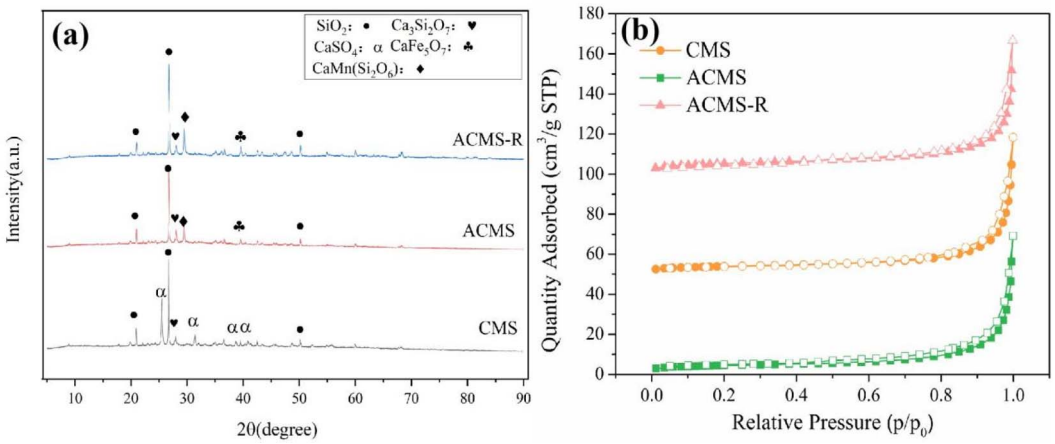

Fig. 3 (a) XRD patterns of CMS, ACMS, and ACMS-R; (b) N_2 adsorption–desorption isotherms of CMS, ACMS, and ACMS-R.

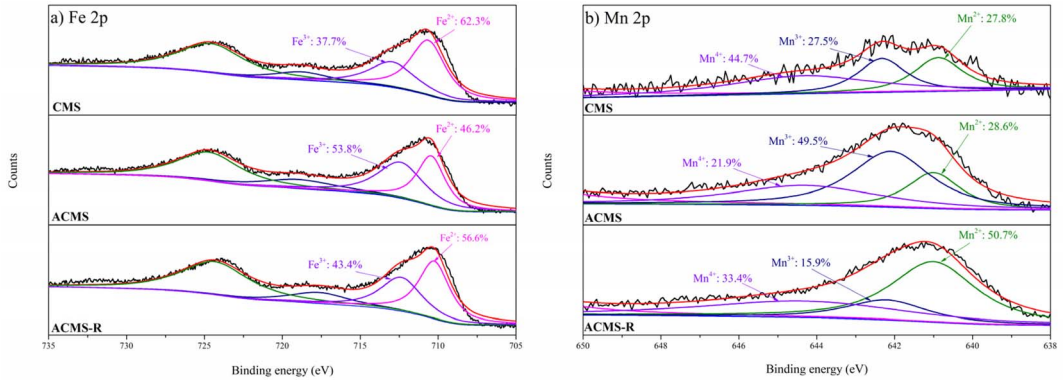

Fig. 4 (a) XPS Fe 2p spectra of CMS, ACMS, and ACMS-R. (b) XPS Mn 2p spectra of CMS, ACMS, and ACMS-R.

than that of CMS, indicating the enhanced performance of ACMS. Treating the sample with alkaline $NaBH_4$ solution further increased the performance since the ACMS-R could remove 65.9% of RhB within 30 min while an even higher removal efficiency of 98.3% could be achieved within 120 min. To clearly evaluate the enhancement of the alkali-reduction treatment by $NaBH_4$ solution, the CMS was also treated by alkaline $NaBH_4$ solution and the obtained CMS-R exhibited poor activity compared to ACMS-R. As shown in Fig. 5b, the calculated RhB degradation kinetics rates for CMS, CMS-R, ACMS, and ACMS-R were 0.014, 0.015, 0.024, and 0.034 min^{-1}, respectively. The RhB degradation kinetics rate of ACMS-R was 2.43 times higher than that of CMS, further indicating the good performance of ACMS-R.

The effects of several parameters on the degradation of RhB with ACMS-R as the catalyst were investigated. RhB removal by PMS activated with ACMS-R as a catalyst under different catalyst dosages was conducted, as depicted in Fig. 6a. When increasing the catalyst dosage from 400 to 800 mg L^{-1}, the RhB removal efficiency increased from 84.3% to 95.2% within 120 min. This could be due to the larger amount of active sites under the higher catalyst dosages. However, further increasing the catalyst dosages to 1200 and 1600 mg L^{-1} resulted in a decrease in the RhB removal efficiency. It has been reported that the degradation of organic pollutants in these system is driven by the active radicals, thus, too high a catalyst dosage might lead to the self-capture of radicals on the surface of the catalyst, resulting in a poorer performance of the catalyst for removing organic pollutants.[9]

It is widely known that the pH value has a significantly influence on the performance of PMS activation. As shown in Fig. 6b, within 30 min, the ACMS-R/PMS system presented RhB removal efficiencies of 38.1%, 46.0%, 58.4%, 49.0%, and 37.5% at pH 3, 5, 7, 9, and 11, respectively. High RhB removal efficiency above 84.3% with pH values ranging from 3 to 11 could be achieved by the ACMS-R/PMS system within 120 min, indicating the effectiveness of ACMS-R. It could be noticed that the highest RhB removal efficiency of 96.0% was achieved at the pH value of 7, while acidic or alkaline conditions slightly hindered the performance of the ACMS-R/PMS system. It is known that the pK_{a2} of PMS is 9.4, which means that the dominant PMS species would be SO_5^{2-} when the pH value is higher than 9.4 (ref. 14). Since SO_5^{2-} is harder to be activated than HSO_5^-, the lower activity under alkaline conditions might be due to this phenomenon.[45] Meanwhile, it has also been reported that H_2SO_5 would be more significant at low pH values and H_2SO_5 is more difficult to activate compared to HSO_5^-, leading to a decrease in performance under acidic conditions.[46]

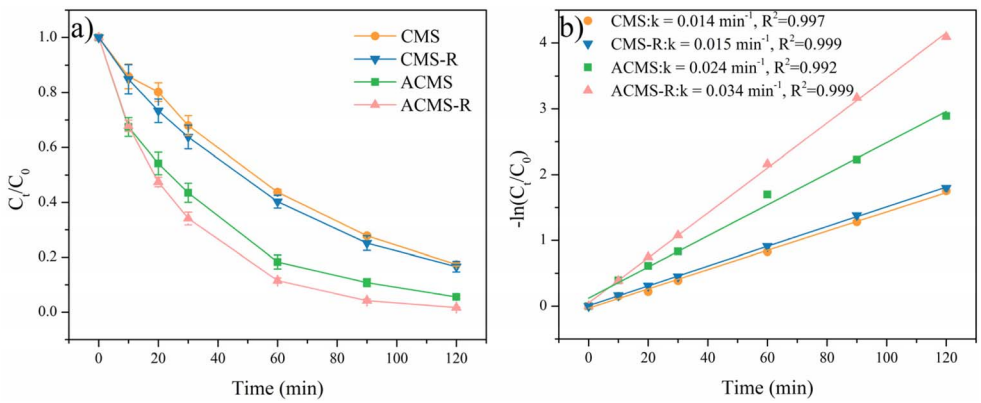

Fig. 5 (a) RhB degradation in PMS activated with the CMS, CMS-R, ACMS, and ACMS-R as catalysts, respectively; (b) corresponding fitted kinetics curves. Experimental conditions: $[RhB]_0$ = 50 mg L^{-1}, [catalyst] = 800 mg L^{-1}, [PMS] = 400 mg L^{-1}, pH_0 = 7, T = 25 °C.

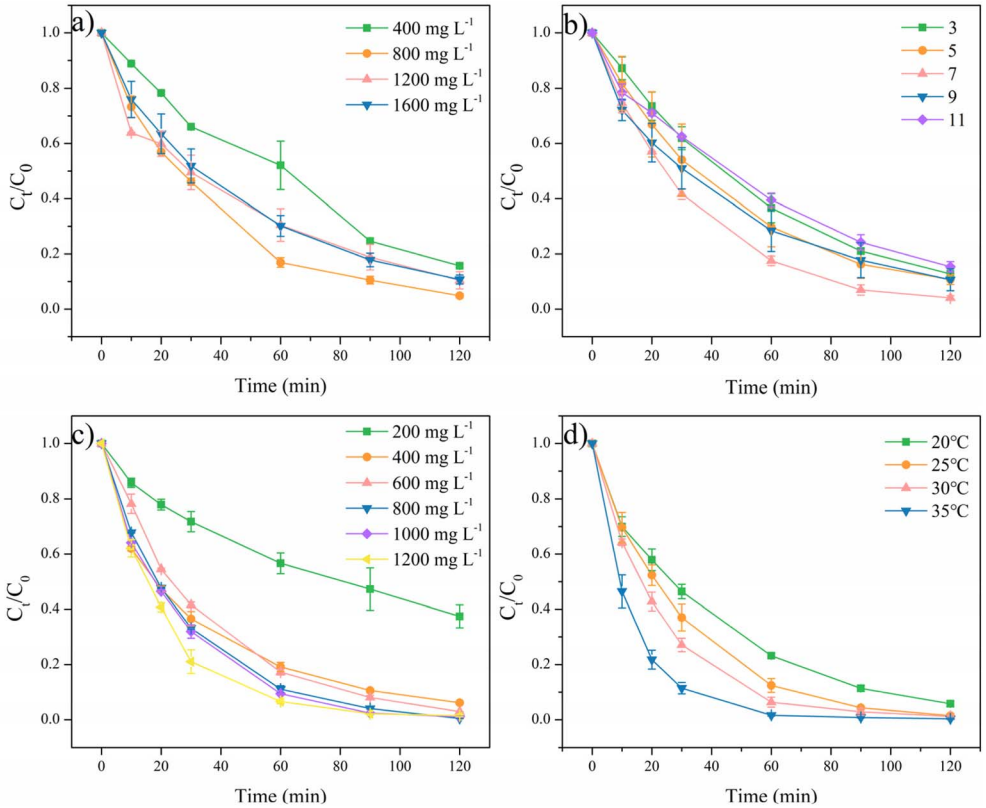

Fig. 6 Effects of the (a) catalyst dosage, (b) pH, (c) PMS concentration, and (d) temperature. Experimental conditions: $[RhB]_0 = 50$ mg L^{-1}, [catalyst] = 800 mg L^{-1} (for b, c, and d), [PMS] = 400 mg L^{-1} (for a and c) and 800 mg L^{-1} for d, $pH_0 = 7$ (for a, b, and d), $T = 25$ °C (for a, b, and c).

Fig. 6c displays the performances at various PMS concentrations. With 200 mg L^{-1} PMS, only 62.6% RhB could be removed within 120 min. The RhB removal efficiencies within 60 min were 43.4%, 80.9%, 82.7%, 89.0%, 90.6%, and 93.4% when the PMS concentrations were 200, 400, 600, 800, 1000, and 1200 mg L^{-1}, respectively, indicating that the RhB removal efficiency increased with increasing the PMS concentration. Significantly, a high RhB removal efficiency of 99.5% could be obtained with 800 mg L^{-1} PMS within 120 min. Nevertheless, further increasing the PMS concentration did not lead to an obvious enhancement of performance, which could be attributed to the self-quenching of PMS.

Based on the above results, the optimized conditions for the ACMS-R/PMS system were revealed to be 800 mg L^{-1} catalyst, 800 mg L^{-1} PMS, and pH 7. The performance of the ACMS-R/PMS system was compared to other systems for RhB degradation, as shown in Table S2†.[47–50] ACMS-R exhibited better activity than other catalysts derived from waste, such as zinc oxide dust and sludge.

Under this condition, the RhB removal was performed at different temperatures (Fig. 6d) and the apparent activation energy (E_a) was calculated according to the Arrhenius equation (eqn (1)):

$$\ln k = \ln A - E_a/RT \quad (1)$$

where k is the apparent first-order rate constant for RhB removal, A is the frequency factor (min^{-1}), R is 8.314 J mol^{-1} k^{-1} and T represents the temperature in Kelvin (K). The calculated results can be seen in Fig. S4† and the E_a for RhB removal by the ACMS-R/PMS system was 33.33 kJ mol^{-1}. An E_a higher than 13.0 kJ mol^{-1} could indicate that the reaction was caused by surface reactions rather than by mass transfer.

3.3 Catalytic mechanism of ACMS-R

The catalytic mechanism of ACMS-R for activating PMS was investigated. Quenching experiments were conducted with adding methanol and L-histidine to identify the reactive oxidative species in the ACMS-R/PMS system. It is known that methanol has a rapid reactive kinetics with both $SO_4^{\bullet-}$ and $^{\bullet}OH$ ($k_{^{\bullet}OH} = 9.7 \times 10^8$ mol L^{-1} s^{-1}, $k_{SO_4^{\bullet-}} = 1.1 \times 10^7$ mol L^{-1} s^{-1}).[34] As shown in Fig. 7a, by adding 0.5 M methanol, 83.0% RhB removal was achieved within 60 min, while that in the control group was 89.0%. The presence of methanol just slightly decreased the RhB removal efficiency, implying that both $SO_4^{\bullet-}$ and $^{\bullet}OH$ did not play vital roles in the degradation of RhB. However, $^1O_2$, which could be generated when the catalysts have oxygen vacancies, has been reported to be effective for removing RhB.[16] Thus, L-histidine was added to capture $^1O_2$ and it was noticed that the RhB removal efficiency significantly decreased to 0% in the presence of 0.05 M L-histidine and 0.5 M methanol. These results indicated that $^1O_2$ played an important role in removing RhB in the ACMS-R/PMS system.

To further demonstrate the generation of $^1O_2$, EPR was employed and the results could be seen in Fig. 7b. Without

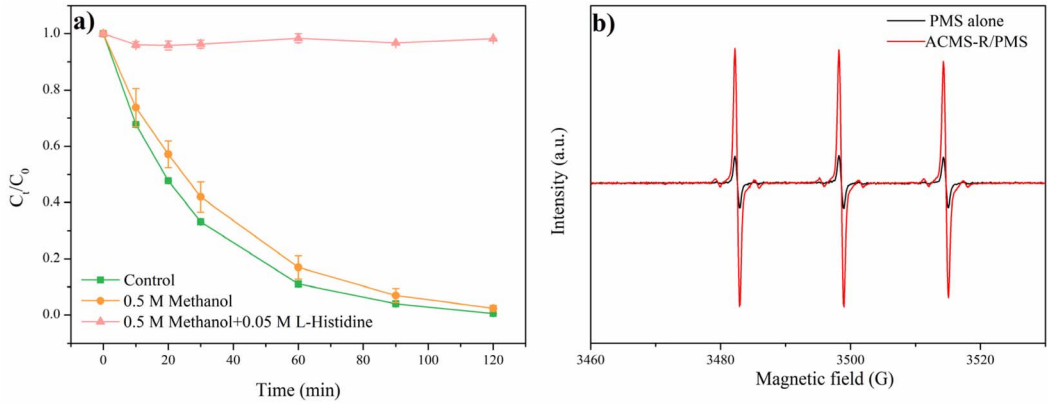

Fig. 7 (a) Quenching experiments with ACMS-R as the catalyst. Experimental conditions: [catalyst] = 800 mg L^{-1}, [PMS] = 800 mg L^{-1}, $[RhB]_0$ = 50 mg L^{-1}, pH = 7, T = 25 °C, [methanol] = 0.5 M, [L-histidine] = 0.05 M. (b) EPR measurements of the ACMS-R/PMS system with TEMP as the spin-trapping agent.

ACMS-R, the solution with PMS alone exhibited the typical triplet peak corresponding to the TEMP-$^1O_2$ adduct.[15] This could be attributed to the reaction between SO_5^{2-} and HSO_5^-, which has been widely reported.[17] Remarkably, after adding the ACMS-R into the PMS solution, the signal increased significantly. These results further indicated the generation $^1O_2$ of in the ACMS-R/PMS system.

The better performance of ACMS-R is further discussed herein. Taking the chemical compositions of ACMS-R into consideration, it is reasonable to speculate that Fe and Mn are the active species. First, the alkali treatment conducted in this study could reduce the content of other inert compositions in the Mn residues, such as Si-based materials, leading to the relatively increased contents of Fe and Mn, as demonstrated by the ICP-AES results. Treating the sample with alkaline $NaBH_4$ solution could introduce more O_V into the sample, and it is reported that the O_V content is correlated to the generation of $^1O_2$. As revealed above, the dominant oxidative species in the ACMS-R/PMS system was $^1O_2$ and the O_V/O_L ratio in ACMS-R was 4.75, which was much higher than that of ACMS (4.14). Thus, the better performance of ACMS-R compared to CMS and ACMS could be attributed to the higher contents of Fe and Mn and the improved content of O_V. To further reveal the chemical conversion during the reaction, the XPS spectrum of ACMS-R after the degradation of RhB was measured and is shown in Fig. 8. The O_V/O_L ratio decreased from 4.75 to 3.12 after the reaction, implying the vital role of oxygen vacancies in the generation of $^1O_2$. As reported in the literature, the weakly-bound oxygen, which is represented by O_V in this manuscript, could be transformed into active oxygen (O*), and the O* could react with HSO_5^- to form $^1O_2$ (eqn (2) and (3)).[12,28] The valence conversion of Fe and Mn during the reaction was also investigated. The relative intensity ratio of Fe^{2+} and Fe^{3+} changed from 56.6 : 43.4 for fresh ACMS-R to 46.1 : 53.9 after the reaction, while those of Mn^{2+}, Mn^{3+}, and Mn^{4+} changed from 50.7 : 15.9 : 33.4 for the initial ACMS-R to 38.5 : 34.6 : 26.9 for the used ACMS-R. These results indicated that both Fe and Mn were involved in the reaction. Since the dominant ROS in the degradation of RhB in the ACMS-R/PMS system was $^1O_2$, it is speculated that the PMS activation mechanism involved the transformation of Mn species from high valence to low valence, which could result in the formation of $SO_5^{\cdot-}$ (eqn (4)–(6)).[44] Consequently, the accumulated $SO_5^{\cdot-}$ could be favorable for the generation $^1O_2$ of through the reaction shown in eqn (7).[37,44] On the other hand, it could be noticed that the low-valence species (Fe^{2+} and Mn^{2+}) increased. This could be attributed to the decreased content of O_V, which need more low-valence metals for coordination.[16,37,51]

$$O_V \rightarrow O^* \quad (2)$$

$$O^* + HSO_5^- \rightarrow HSO_4^- + {}^1O_2 \quad (3)$$

$$\equiv Mn(IV) + HSO_5^- \rightarrow \equiv Mn(III) + SO_5^{\cdot-} + H^+ \quad (4)$$

$$\equiv Mn(III) + HSO_5^- \rightarrow \equiv Mn(II) + SO_5^{\cdot-} + H^+ \quad (5)$$

$$\equiv Fe(III) + HSO_5^- \rightarrow \equiv Fe(II) + SO_5^{\cdot-} + H^+ \quad (6)$$

$$2SO_5^{\cdot-} + 2H_2O \rightarrow 4H^+ + 2SO_4^{2-} + 2{}^1O_2 \quad (7)$$

3.4 Applicability and reusability of ACMS-R

As the catalyst was prepared using solid waste as precursors, the applicability and reusability of ACMS-R are very important. Anion substances widely exist in actual water bodies and could influence the PMS activation performance. As shown in Fig. 9a, with the presence of 25 mmol per L Cl^- or 25 mmol per L $H_2PO_4^-$, the RhB removal efficiencies in the ACMS-R/PMS system within 60 min were 98.2% and 93.0%, respectively. Both of those were slightly higher than that of the control group (89.0%). These results demonstrated the good performance of ACMS-R in complex water bodies with different anions.

Next, the stability of ACMS-R was investigated and the results are presented in Fig. 9b. After five cycles under the same conditions, a high RhB removal efficiency of 94.4% could still be

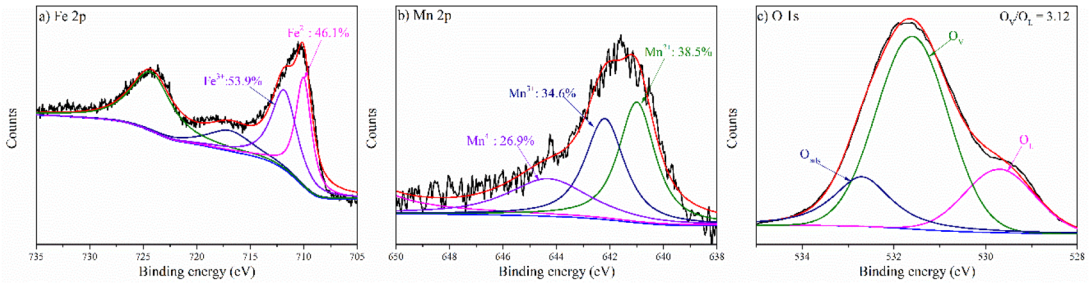

Fig. 8 (a) XPS Fe 2p, (b) Mn 2p, and (c) O 1s spectra of ACMS-R after the reaction.

achieved within 120 min, indicating the good reusability of ACMS-R.

To further reveal the performance of ACMS-R in real water in actual water bodies, two typical actual water body samples were gathered for conducting the RhB degradation experiments. River water was collected from the Yangtze River and lake water was obtained from Cuihu Lake in the campus of Chongqing Technology and Business University. First, 50 mg L^{-1} RhB was added in to these water body samples and the pH was adjusted to 7 before the reaction. As depicted in Fig. S5,† within 60 min, the ACMS-R/PMS system could remove 98.7% of the RhB in the lake water and 97.5% of the RhB in the river water. These results demonstrated that ACMS-R has excellent activity for RhB degradation in actual water bodies.

3.5 Major degradation intermediates

To comprehensively elucidate the potential degradation mechanisms of RhB, LC-MS was employed for analysis of the degradation intermediates. The corresponding mass data are presented in Table S3,† with a comprehensive list of the intermediates encountered along the RhB degradation pathway. Based on the detected intermediates, the RhB degradation pathway was constructed (Fig. 10). The experimental results demonstrated that the degradation of RhB involved a complex interplay of various chemical reactions, encompassing deethylation, deamination, dealkylation, decarboxylation, chromophore cleavage, ring-opening, and ultimate mineralization.[52] At the initial stage of degradation, oxidative species primarily targeted the C=N bond, initiating a deethylation reaction, which transformed RhB (m/z = 443) into P1, P2, and P3 (m/z = 387).[53] Subsequently, the continued action of the oxidative species progressively removed the ethyl groups from these intermediates, sequentially yielding P4, P5 (m/z = 359), and ultimately P6 (m/z = 331) upon detachment of the final ethyl group. Following the rupture of the –NH_3 bond, P6 was transformed into P7 (m/z = 301).[52] Furthermore, the central carbon atom of P7 was attacked, leading to the formation of P8 (m/z = 269), P9 (m/z = 279), P10 (m/z = 283), P11 (m/z = 214), and P12 (m/z = 182).[48] As degradation progressed, the chromophore structure underwent disruption, resulting in the formation of a series of monocyclic aromatic compounds, including P13 (m/z = 154), P14 (m/z = 122), and P15 (m/z = 94).[54] Subsequently, oxidative species persisted in the oxidation process, catalyzing the ring–opening reactions of the macromolecular organic intermediates, giving rise to alcohols and acids, such as P16 (m/z = 90), P17 (m/z = 90), and P18 (m/z = 116).[54] The final stage of degradation involved mineralization, where the alcohols and acids were thoroughly decomposed into small inorganic molecules, including NO_3^-, NH_4^+, CO_2, and H_2O.[52,55] To demonstrate the mineralization of RhB during the reaction, TOC values were measured, as shown in Fig. S6.†

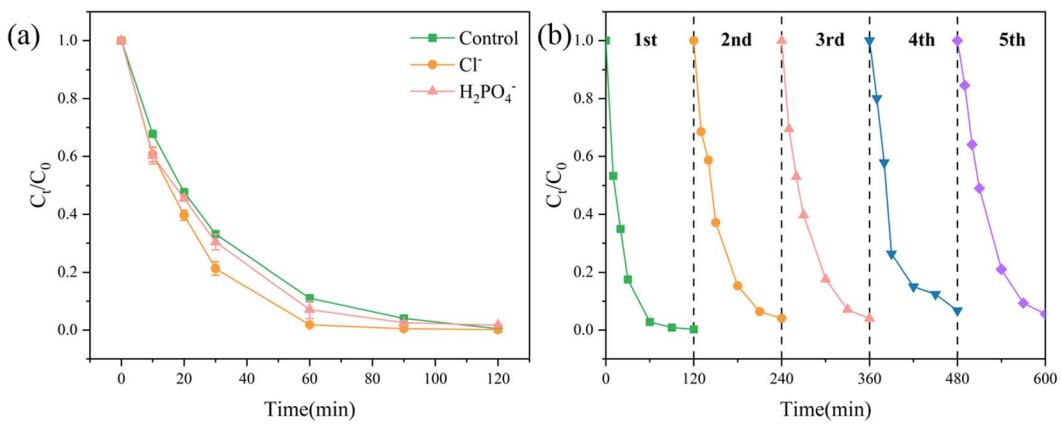

Fig. 9 (a) Effects of Cl^- and $H_2PO_4^-$ on RhB degradation by the ACMS-R/PMS system. Experimental conditions: $[RhB]_0$ = 50 mg L^{-1}, [catalyst] = 800 mg L^{-1}, [PMS] = 800 mg L^{-1} [anions] = 25 mmol L^{-1}, pH = 7, T = 25 °C. (b) Stability experiments of ACMS-R. Experimental conditions: $[RhB]_0$ = 50 mg L^{-1}, [catalyst] = 800 mg L^{-1}, [PMS] = 800 mg L^{-1}, pH = 7, T = 25 °C.

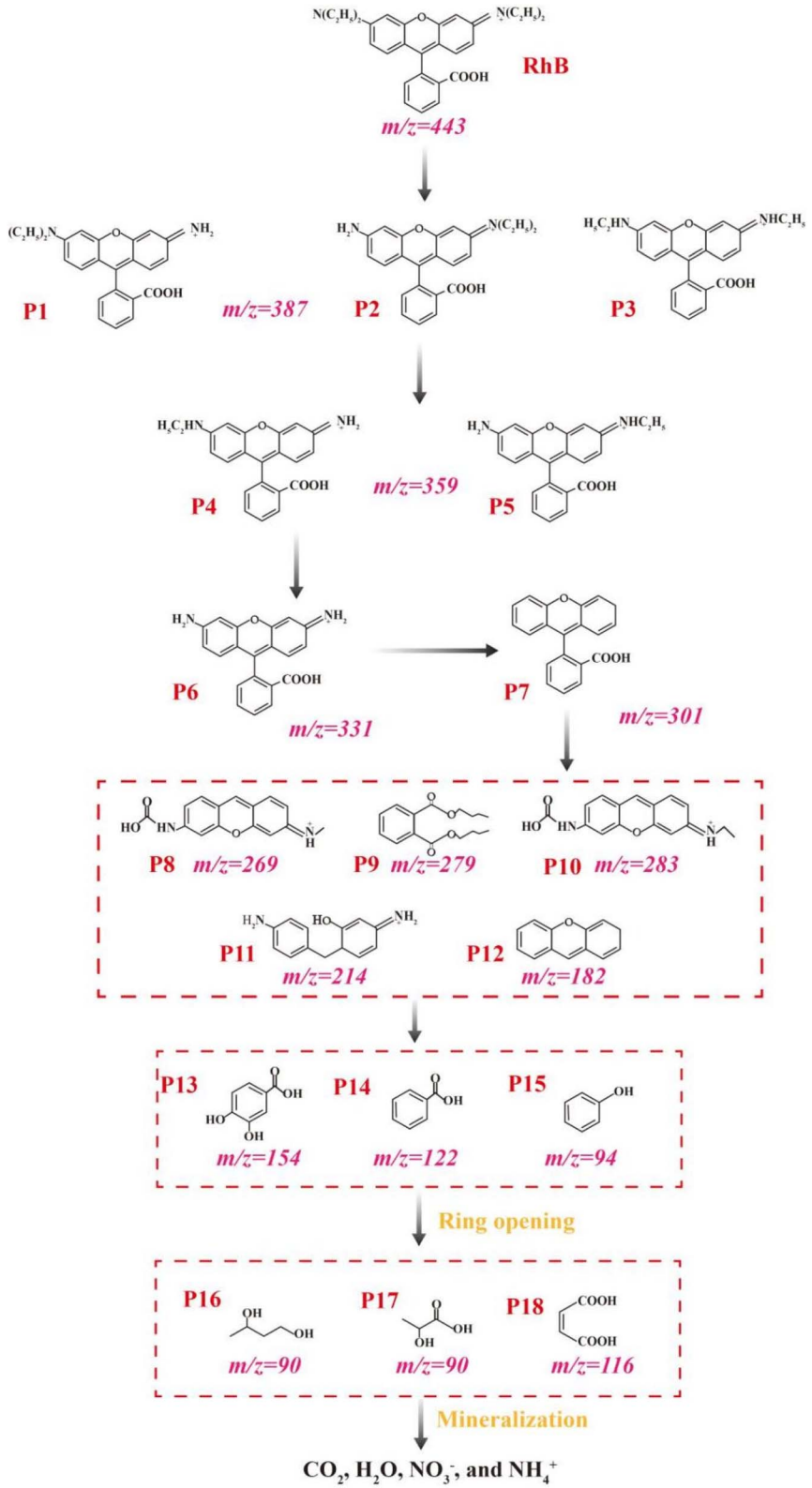

Fig. 10 Possible RhB degradation pathways in the ACMS-R/PMS system.

Within 120 min, the TOC removal efficiency reached 24.2% in the ACMS-R/PMS system, indicating the mineralization of RhB by PMS activated with ACMS-R as the catalyst.

3.6 Toxicity assessment

To evaluate the environmental implications, a quantitative structure–activity relationship (QSAR) approach was employed

to utilize the toxicity estimate software tool (T.E.S.T.) to conduct toxicity analysis and predict the toxicity changes during the RhB degradation process. Specifically, the fathead minnow LC_{50} (96 h), daphnia magna LC_{50} (48 h), oral rat LD_{50}, bioconcentration factor, developmental toxicity, and mutagenicity were investigated.[56] The results are presented in Fig. S7 and Table S4.† The LC_{50} (96 h), LC_{50} (48 h), developmental toxicity, and mutagenicity of RhB were determined to be 0.04 mg L^{-1}, 4.63 mg L^{-1}, 0.95, and 0.26, respectively, predicting it as "very toxic," "toxic," and "developmentally toxic".[56] For fathead minnows (Fig. S7a†), all the intermediates exhibited lower toxicity than RhB. For the daphnia magna (Fig. S7b†), only intermediates P11 (1.87 mg L^{-1}) and P12 (1.92 mg L^{-1}) surpassed the toxicity of RhB. For oral rat (Fig. S7c†), most intermediates displayed lower toxicity than RhB (924.86 mg kg^{-1}). Regarding the bioaccumulation factors (Fig. S7d†), only the intermediate P7 (27.57) had a higher bioconcentration factor than RhB (15.48). In terms of the developmental toxicity (Fig. S7e†), most intermediates were less toxic than RhB (0.95). For mutagenicity (Fig. S7f†), the intermediates of the terminal degradation pathways exhibited low mutagenicity, classified as "mutagenicity negative".[56] In summary, despite a few intermediates, like, P2 exhibiting higher toxicity than RhB, the majority of the intermediates presented lower toxicity, indicating that RhB could be oxidized into less toxic products in the ACMS-R/PMS system.

4. Conclusions

A two-step method involving alkali treatment and $NaBH_4$ alkali-reduction treatment was developed to transform Mn residues into catalysts for activating PMS toward the degradation of RhB with good performance. The alkali treatment removed the Si and prevented the leaching of Fe and Mn, which are regarded as the active species. The alkaline $NaBH_4$ solution treatment successfully increased the content of oxygen vacancies. The optimized catalyst presented good performance with $^1O_2$ as the dominant ROS. Overall, 18 kinds of degradation intermediates were revealed and the possible degradation pathways were proposed. Toxicity assessment by T.E.S.T. demonstrated the significantly decreased toxicity during the degradation of RhB. Furthermore, the ACMS-R/PMS system was effective when tested with water samples from actual water bodies, such as lake water and river water, and the system also exhibited high reusability during five recycles.

Data availability

The authors do not have permission to share data.

Conflicts of interest

The authors declare that they have no known competing financial interests or personal relationships that could have appeared to influence the work reported in this paper.

Acknowledgements

This work was supported by the National Natural Science Foundation of China [grant number 52300032], Natural Science Foundation of Chongqing [grant numbers CSTB2023NSCQ-MSX0700, CSTB2023NSCQ-MSX0789, and CSTB2024NSCQ-MSX1255], Chongqing Municipal Education Commission [grant numbers KJQN202300838, KJZD-M202200802, KJQN202201548, KJQN202401554, and KJQN202401548] and Start-up Foundation of High-level Talents in Chongqing Technology and Business University [grant number 2356017].

References

1 F. Wang, G. Long, K. Ma, X. Zeng, Z. Tang, R. Dong, J. He, M. Shangguan, Q. Hu, R. K. Liew, Y. Li and J. Zhou, *Environ. Chem. Lett.*, 2023, **21**, 2251–2284.
2 H. Su, W. Zhou, X. Lyu, X. Liu, W. Gao, C. Li and S. Li, *Miner. Eng.*, 2023, **202**, 108264.
3 R. Ji, T.-J. Liu, L.-L. Kang, Y.-T. Wang, J.-G. Li, F.-P. Wang, Q. Yu, X.-M. Wang, H. Liu, H.-W. Guo, W.-L. Xu, Y.-N. Zeng and Z. Fang, *J. Clean. Product.*, 2022, **380**, 135076.
4 F. Wang, G. Long and J. L. Zhou, *J. Hazard. Mater.*, 2024, **465**, 133419.
5 F. Wang, G. Long and J. L. Zhou, *Sci. Total Environ.*, 2023, **894**, 165049.
6 J. Shu, Y. Deng, X. Wei, M. Chen, Y. Yang and Z. Deng, *ACS ES&T Water*, 2023, **3**, 2229–2237.
7 X. Li, H. Liu, Y. Zhang, J. Mahlknecht and C. Wang, *J. Environ. Manage.*, 2024, **352**, 120051.
8 C. Chen, L. Liu, W. Li, Y. Lan and Y. Li, *J. Hazard. Mater.*, 2022, **439**, 129572.
9 S. Sun, S. Song, S. Yang, Y.-L. He, Y. Shi, P. Zhou, Z.-k. Xiong, Y. Liu, H. Zhang, Y. Du, C.-S. He and B. Lai, *Chin. Chem. Lett.*, 2024, **35**, 109242.
10 Z. Ha, M. Ma, X. Tan, Y. Lan, Y. Lin, T. C. Zhang and D. Du, *Environ. Res.*, 2023, **234**, 116607.
11 A. Xu, S. Fan, T. Meng, R. Zhang, Y. Zhang, S. Pan and Y. Zhang, *Appl. Catal., B*, 2022, **318**, 121833.
12 Y. Chen, X. Bai, Y. Ji and D. Chen, *J. Hazard. Mater.*, 2023, **441**, 129912.
13 Q. He, X. Liao, G. Li, Y. He and J. Shen, *Chem. Phys.*, 2023, **571**, 111912.
14 S. Zhu, H. Li, L. Wang, Z. Cai, Q. Wang, S. Shen, X. Li and J. Deng, *Chem. Eng. J.*, 2023, **458**, 141415.
15 J. Yan, L. Gong, S. Chai, C. Guo, W. Zhang and H. Wan, *Chem. Eng. J.*, 2023, **458**, 141456.
16 J. Zhao, F. Li, H. Wei, H. Ai, L. Gu, J. Chen, L. Zhang, M. Chi and J. Zhai, *Chem. Eng. J.*, 2021, **409**, 128150.
17 Z. Yang, X. Tan and C. Zhang, *Sep. Purif. Technol.*, 2024, **336**, 126320.
18 L. Zhao, J. Zhang, Z. Zhang, T. Wei, J. Wang, J. Ma, Y. Ren and H. Zhang, *J. Colloid Interface Sci.*, 2022, **623**, 520–531.
19 W. Chen, X. Guo, M. Wu, Z. Liu, C. Yang, H. Xie and J. Chen, *Sep. Purif. Technol.*, 2024, **335**, 126263.
20 W. Zhou, M. Li and Y. Liu, *J. Environ. Manage.*, 2024, **351**, 119876.

21 M. Li, Y. Zhang, Y. Liu, Y. Chen, Z. You, L. Zhang, Y. Liang and Z. He, *J. Clean. Product.*, 2023, **428**, 139408.
22 X. Zhou, Y. Wang, X. Wang and Y. Zhang, *J. Environ. Chem. Eng.*, 2023, **11**, 110120.
23 M. Wu, W. Sun, X. Meng, J. Kang and Y. Yang, *ACS ES&T Water*, 2023, **3**, 3265–3273.
24 M. Li, Z. He, H. Zhong, W. Sun, M. Ye and Y. Tang, *J. Environ. Manage.*, 2023, **328**, 116945.
25 M. Li, Z. He, H. Zhong, L. Hu and W. Sun, *Environ. Sci.: Nano*, 2022, **9**, 1037–1051.
26 H. Liang, W. Wang, W. Liang, X. Deng, X. Ruan, D. Zhang and Y. Yang, *J. Environ. Chem. Eng.*, 2023, **11**, 109126.
27 C. Quimbaya-Ñañez, E. A. Serna-Galvis, J. Silva-Agredo, L. Huerta, R. A. Torres-Palma and Y. Ávila-Torres, *J. Environ. Chem. Eng.*, 2024, **12**, 112015.
28 M. Li, Z. He, H. Zhong, W. Sun, L. Hu and M. Luo, *Chem. Eng. J.*, 2022, **441**, 136024.
29 H. Shen, M. Luo, J. Wang, M. Li, Z. He, H. Zhong, W. Sun, M. Ye and Y. Tang, *Chem. Eng. J.*, 2023, **472**, 144915.
30 M. Li, H. Zhong, Z. He, L. Hu, W. Sun, P. Loganathan and D. Xiong, *Chem. Eng. J.*, 2021, **413**, 127478.
31 M. Li, F. Huang, L. Hu, W. Sun, E. Li, D. Xiong, H. Zhong and Z. He, *Chem. Eng. J.*, 2020, **401**, 126085.
32 X. Zhou, C. Luo, J. Wang, H. Wang, Z. Chen, S. Wang and Z. Chen, *Sci. Total Environ.*, 2021, **762**, 143120.
33 J. Ni, Q. Zhang, X. Fu, Q. Zhang, S. Wu, Z. Xiong, J. Wang and Q. Zeng, *ACS Appl. Nano Mater.*, 2023, **6**, 13492–13502.
34 J. Liang, M. Guo, Y. Xue, J.-n. Gu, J. Li, F. Shi, X. Guo, X. Min, J. Jia, K. Li and T. Sun, *Chem. Eng. J.*, 2022, **435**, 135000.
35 C. Pan, Y. Sun, Y. Dong, H. Hou, M. F. Kai and J. Lan, *J. Hazard. Mater.*, 2024, **465**, 133198.
36 Z. Yang, Z. Zhou, X. Tan, G. Zeng and C. Zhang, *J. Mater. Sci. Technol.*, 2025, **204**, 224–237.
37 Y. Guan, G. Zhou, L. Li, Y. Jiang, J. Yin, C. Liu, L. Zhang, Q. Han and E. H. Ang, *Sep. Purif. Technol.*, 2024, **335**, 126072.
38 T. C. Khiem, N. N. Huy, E. Kwon, S. Wacławek, A. Ebrahimi, W.-D. Oh, S. Ghotekar, Y. F. Tsang, W.-H. Chen and K.-Y. A. Lin, *Chem. Eng. J.*, 2023, **476**, 146404.
39 A. Khan, H. Ullah, Q. Wu, W. Gong, L. Ma, S. Zhao, A. Xu and X. Li, *Chem. Eng. J.*, 2023, **472**, 145112.
40 M. Xu, Q. Zhang, Z. Zhu, Y. Xue, T. Zhang and J. Hong, *J. Clean. Product.*, 2022, **377**, 134258.
41 Y. Zhao, L. Wu, P. Hong, X. He, S. Gao, Y. Yu, B. Liao and H. Pang, *Appl. Surf. Sci.*, 2024, **645**, 158864.
42 L. Yu, G. Zhang, C. Liu, H. Lan, H. Liu and J. Qu, *ACS Catal.*, 2018, **8**, 1090–1096.
43 C. Gong, F. Chen, Q. Yang, K. Luo, F. Yao, S. Wang, X. Wang, J. Wu, X. Li, D. Wang and G. Zeng, *Chem. Eng. J.*, 2017, **321**, 222–232.
44 M. Chen, T. Yang, L. Zhao, X. Shi, R. Li, L. Ma, Y. Huang, Y. Wang and S.-c. Lee, *Appl. Surf. Sci.*, 2024, **645**, 158835.
45 X. Duan, C. Su, J. Miao, Y. Zhong, Z. Shao, S. Wang and H. Sun, *Appl. Catal., B*, 2018, **220**, 626–634.
46 J. Huang, Y. Dai, K. Singewald, C.-C. Liu, S. Saxena and H. Zhang, *Chem. Eng. J.*, 2019, **370**, 906–915.
47 X. Shan, Z. Xie, X. Ma, Y. Xu, S. Zhang, Q. Jia, R. Wan and H. Tao, *Microporous Mesoporous Mater.*, 2022, **337**, 111948.
48 Y. Huang, X. Chen, Y. Fan, C. Wang, Y. Cao, W. Peng, B. Fu, J. Liu and M. Hu, *Miner. Eng.*, 2024, **214**, 108781.
49 Z. Huang, T. Wang, M. Shen, Z. Huang, Y. Chong and L. Cui, *Chem. Eng. J.*, 2019, **369**, 784–792.
50 L. Zheng, S. Cao, M. Tang and M. Ge, *Water, Air, Soil Pollut.*, 2025, **236**, 65.
51 G. Fang, J. Zhou, Y. Cai, S. Liu, X. Tan, A. Pan and S. Liang, *J. Mater. Chem. A*, 2017, **5**, 13983–13993.
52 Y. Ren, J. Wang, G. Qu, N. Ren, P. Lu, X. Chen, Z. Wang, Y. Yang and Y. Hu, *Sep. Purif. Technol.*, 2023, **314**, 123616.
53 H. Cheng, X. Li, C. Huang, J. Zhu, P. Wang, H. Cao, C. Feng, D. Ling, H. Liu and M. Cheng, *J. Clean. Product.*, 2023, **393**, 136354.
54 T. Xu, L. Fu, H. Lu, M. Zhang, W. Wang, B. Hu, Y. Zhou and G. Yu, *J. Clean. Product.*, 2023, **401**, 136794.
55 J. Zhang, M. Yan, G. Sun, X. Li, B. Hao and K. Liu, *Chemosphere*, 2022, **304**, 135318.
56 Y. Liu, X. Zhang, X. Li and Z. Zhou, *J. Water Process Eng.*, 2024, **57**, 104588.